

Hyperfine Interactions in Graphene and Related Carbon Nanostructures

Oleg V. Yazyev*

*Ecole Polytechnique Fédérale de Lausanne (EPFL),
Institute of Chemical Sciences and Engineering, CH-1015 Lausanne, Switzerland*

(Dated: February 8, 2020)

Hyperfine interactions, magnetic interactions between the spins of electrons and nuclei, in graphene and related carbon nanostructures are studied. By using a combination of accurate first principles calculations on graphene fragments and statistical analysis, I show that both isotropic and dipolar hyperfine interactions can be accurately described in terms of the local electron spin distribution and atomic structure. A complete set of parameters describing the hyperfine interactions of ^{13}C and other nuclear spins at substitution impurities and edge terminations are determined.

PACS numbers: 75.75.+a, 81.05.Uw

Graphene and related carbon nanostructures are considered as potential building blocks of future electronics, including spintronics [1] and quantum information processing based on electron spins [2] or nuclear spins [3]. Carbon nanostructures are attractive for these applications because of the negligible spin-orbit coupling in materials made of light elements [4, 5]. Promising results for the spin-polarized current lifetimes in carbon nanotubes [6, 7, 8] and graphene [9] unambiguously confirm the potential of these materials. A number of quantum dot devices, components of solid-state quantum computers, based on carbon nanostructures have been proposed recently [10, 11, 12, 13]. Hyperfine interactions (HFIs), the magnetic interactions between the spins of electrons and nuclei, are expected to be the leading contribution to the spin decoherence in carbon materials [4, 7, 14]. Minimizing HFIs with nuclear spins is necessary for achieving longer electron spin coherence times [15], while in some other instances the HFIs play an important role as a link between the spins of electrons and nuclei in the system [3, 16, 17, 18]. A common understanding of hyperfine interactions is thus necessary for engineering future electronic devices based on graphene and related nanostructures.

In this Letter, I study the hyperfine interactions in graphene nanostructures by using a combination of accurate first principles calculations on graphene fragments and statistical analysis. I show that the interaction of the conduction π electron spins with nuclear spins can be described in terms of only the local (on-site and first-nearest-neighbor) electron spin distribution and the local atomic structure. In many practical situations, the former can be found using simpler computational approaches, e.g. tight binding or analytical approximations. The local nature of HFIs justifies the extension of my results from small molecular models to extended systems. I further extend the considerations to curved topologies and to the presence of heteronuclei at impurities and boundaries.

The all-electron DFT calculations [19] were performed using a combination of the EPR-III Gaussian orbital ba-

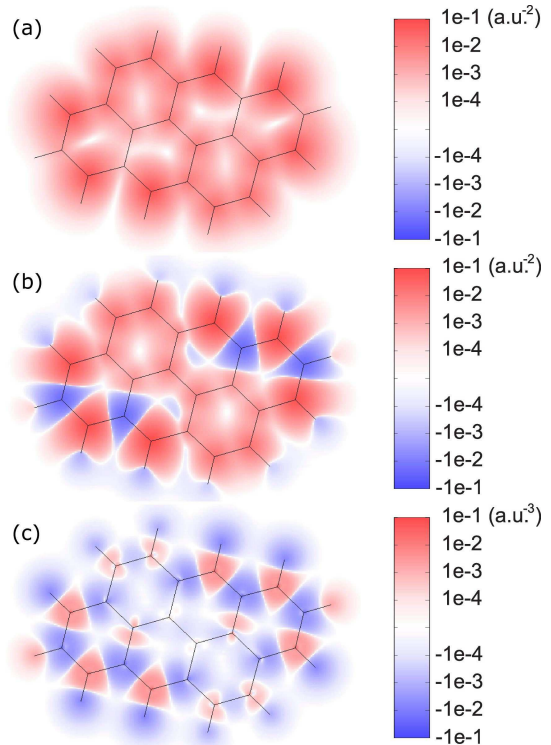


FIG. 1: (Color online). Projections of the spin-polarized conduction electron density $\rho_c^s(\mathbf{r})$ (a) and the total spin density $\rho^s(\mathbf{r})$ (b) on the plane of a small nanographite molecule in its triplet spin state. The magnitudes of the total spin density $\rho^s(\mathbf{r}, z=0)$ (c) in the plane of nuclei reflects the isotropic hyperfine field. Molecular framework is shown by black lines.

sis set [20] specially tailored for the calculations of hyperfine couplings and the B3LYP exchange-correlation hybrid density functional [21]. This computational protocol can be applied to molecules of limited size and predicts hyperfine coupling constants (HFCCs) in excellent agreement with experimental results [22]. For a set of representative experimentally measured ^{13}C isotropic HFCCs of small graphenic ion-radicals [23] our computations provide a mean absolute error of 1.1 MHz ($\approx 2\%$ of the range of magnitudes), which justifies the use of

calculated HFCCs as a reference.

The Hamiltonian of the HFI between the electron spin \mathbf{S} and the nuclear spin \mathbf{I} can be written as $\hat{\mathbf{H}}=\mathbf{S}\cdot\hat{\mathbf{A}}\cdot\mathbf{I}$, where the 3×3 HFI tensor $\hat{\mathbf{A}}=A_{iso}\cdot\hat{\mathbf{1}}+\hat{\mathbf{T}}$ is usually decomposed into the scalar HFCC A_{iso} and the traceless dipolar HFI tensor $\hat{\mathbf{T}}$. The HFI tensor $\hat{\mathbf{A}}$ reflects the distribution of the electron spin density $\rho^s(\mathbf{r})=\rho^{\uparrow}(\mathbf{r})-\rho^{\downarrow}(\mathbf{r})$ viewed from the position of the nucleus I . In carbon nanostructures the nuclear spins are those of the ^{13}C isotope ($\sim 1.1\%$ natural abundance and can be artificially changed; the dominant ^{12}C isotope has zero spin) and other elements originating from impurities and boundaries. The electron spin density $\rho^s(\mathbf{r})$ can be further decomposed into the contribution of half-populated conduction electron states lying close to the Fermi level (or singly occupied molecular orbitals in the molecular context), $\rho_c^s(\mathbf{r})=\sum_c|\psi^c(\mathbf{r})|^2\geq 0$, and the contribution of the fully populated valence states perturbed by the spin-polarized conduction electrons, $\rho_v^s(\mathbf{r})=\sum_v|\psi^{v\uparrow}(\mathbf{r})|^2-|\psi^{v\downarrow}(\mathbf{r})|^2$. The spin-polarization of the valence electrons is illustrated with a model hydrogen-terminated graphene fragment in the triplet spin state (Fig. 1). While the projection of $\rho_c^s(\mathbf{r})$ on the xy plane (Fig. 1a) is positive everywhere and reveals an enhancement at the zig-zag edges, the projection of the total spin-density $\rho(\mathbf{r})$ (Fig. 1b) is negative where $\rho_c^s(\mathbf{r})$ is close to zero. The isotropic (Fermi contact) HFCC is proportional to the total spin density at the position of nuclear spin I , $A_{iso}=\frac{8\pi}{3}\gamma_e\gamma_I\hbar^2\rho(\mathbf{r}_I)$, where γ_e and γ_I are the electron and nuclear gyromagnetic ratios, respectively. For the ideal graphene and planar sp^2 carbon nanostructures (all nuclei lie in the $z=0$ plane) $\rho_c^s(z=0)=0$ due to the p_z symmetry of the conduction states. However, there is a contribution of the σ symmetry valence states $\rho_v^s(z=0)\neq 0$ due to the spin-polarization effect. For the model graphene fragment $\rho_v^s(z=0)$ (Fig. 1c) shows an alternating pattern with a relative dominance of the negative spin density. Since the σ states are situated well above and well below the Fermi level in sp^2 carbon nanostructures, the valence spin-polarization phenomenon exhibits the property of locality. This property has been exploited by Karplus and Fraenkel almost 50 years ago to describe the isotropic ^{13}C HFCCs in conjugated organic radicals [24]. The main contribution to the hyperfine anisotropy originates from the total spin population n of the on-site p_z atomic orbital, which also incorporates the contribution of spin-polarized valence states. Assuming a local axial symmetry, $\hat{\mathbf{T}}$ can be written as a diagonal matrix with elements $T_{zz}/2=-T_{xx}=-T_{yy}=A_{dip}$, where $A_{dip}=\frac{2}{5}\gamma_e\gamma_I\hbar^2n\langle 1/r_{2p}^3 \rangle$ (r_{2p} is the distance of the carbon $2p$ electron to nucleus).

The HFIs in planar graphene fragments were calculated for a set of 12 small planar hydrogen terminated nanographites (Fig. 2a) in the triplet spin states. This provides an overall statistics of 103 inequivalent ^{13}C

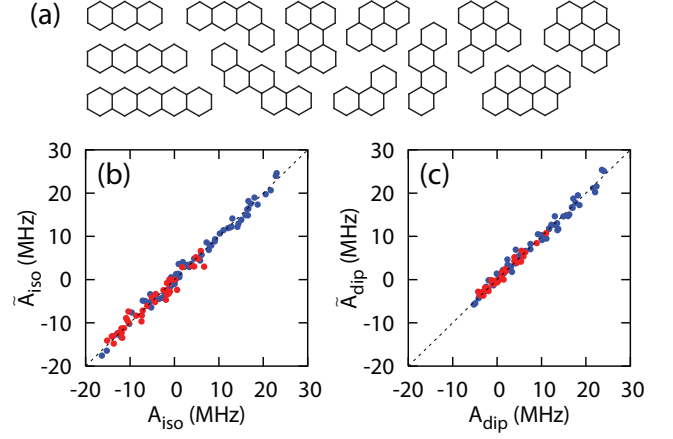


FIG. 2: (Color online) (a) Set of graphene fragments used in the present calculations. Predicted Fermi contact (\tilde{A}_{iso}) and dipolar (\tilde{A}_{dip}) ^{13}C HFCCs vs the corresponding values, A_{iso} (b) and A_{dip} (c), calculated from first principles. The values for inner (3 carbon NNs) and boundary (2 carbon NNs) atoms are shown as red and blue dots, respectively.

TABLE I: Parameters (in MHz) fitted to the results of calculations of a set of nanographite molecules.

	a_2	a_3	b_2	b_3	c	d
A_{iso}	151	135	1.7	4.9	-57.6	-5.5
A_{dip}	144	116	2.9	5.2	-17.3	-13.9

HFCCs. The calculated A_{iso} and A_{dip} values are fitted to the extended form of the Karplus-Fraenkel expression

$$A = a_j(1 + \sum_{i \in NN} b_j \Delta r_i) n^c + c \sum_{i \in NN} (1 + d \Delta r_i) n_i^c, \quad (1)$$

where the two terms account for the contributions of the on-site and nearest neighbor (NN) conduction electron spin populations, n^c and n_i^c , respectively, calculated from first principles. The on-site coefficients a_j and b_j are distinguished for the cases of C atoms with 3 carbon NNs ($j=3$) and the boundary atoms with 2 carbon NNs ($j=2$). The C–C bond length effects are encountered through the coefficients b_j and d with $\Delta r_i = r_i - r_0$ being the deviation of the bond length r_i from the value for the ideal graphene, $r_0 = 1.42 \text{ \AA}$. The results of the regressions are summarized in Tab. I (1 MHz = $4.136 \times 10^{-3} \text{ \mu eV}$). Fig. 2(b,c) shows the predicted (using expression (1) and fitted parameters) values \tilde{A}_{iso} (\tilde{A}_{dip}) versus the calculated A_{iso} (A_{dip}) values. Regressions to the linear expression (1) provide accurate (root-mean-square-errors are 1.2 MHz and 1.8 MHz for A_{iso} and A_{dip} , respectively) and unbiased estimations. The calculated isotropic HFCCs span about the same range of magnitudes ($-16.3 \text{ MHz} < A_{iso} < 23.1 \text{ MHz}$) as the dipolar HFCCs ($-5.3 \text{ MHz} < A_{dip} < 24.1 \text{ MHz}$). The HFCCs of boundary atoms tend to be larger due to the fact that low-energy states localize at the zigzag graphene edges

[25]. The on-site and the NN spin-polarization effects have competitive character ($a_3/c \approx -2.5$) in the case of isotropic HFCCs. Our calculations predict $\approx 50\%$ larger values for the parameters a_2 , a_3 and c for A_{iso} compared to those obtained by Karplus and Fraenkel in their early studies of HFCCs in molecular radicals ($a_2=99.8$ MHz, $a_3=85.5$ MHz and $c=-39$ MHz) [24]. This difference can be explained by the explicit incorporation of the electron correlation effects in our calculations and to the characteristic local atomic structure of the graphene lattice. Both A_{iso} and A_{dip} show a tendency to enhance the on-site and to weaken the NN contributions with the increase of C–C bond lengths. The dipolar HFCC is mostly influenced by the on-site contribution of the half-populated conduction state and the NN spin-polarization effect is weaker in this case ($a_3/c \approx -7$). When compared to typical solid state environments based on heavier elements, the ^{13}C HFCCs in graphene and related nanostructures are weaker (e.g. 117 MHz ^{31}P Fermi contact HFCC for the P shallow donor in Si [26]) and more anisotropic.

The graphene honeycomb lattice is a bipartite lattice, i.e. can be partitioned into two complementary sublattices A and B . I discuss the HFIs for the three general cases of conduction electron spin distributions over the sublattices: (i) ferromagnetic $n_A^c=n_B^c>0$; (ii) ferrimagnetic $n_A^c>0$ and $n_B^c=0$ and (iii) antiferromagnetic $n_A^c=-n_B^c>0$ (see Tab. II). The first case can be physically realized upon the uniform magnetization of the system with equivalent A and B sublattices, e.g. by applying an external magnetic field. The negative $A_{iso}=-35.8$ MHz is small due to the partial compensation of the on-site and the NN spin-polarization effects. This value is consistent with the values derived from the experimental ^{13}C Knight shifts in graphite intercalates (-25 MHz $< A_{iso} < -50$ MHz) [27] and with the calculated isotropic Knight shifts in metallic carbon nanotubes [28]. The ferrimagnetic case with the conduction state distributed over the atoms of only one sublattice (A) is physically realized at the zigzag edges [25] and around single-atom point defects in sublattice B [29]. Considerable alternating Fermi contact and dipolar HFCCs are predicted in this case. An antiferromagnetic pattern can be realized in the case of heavily disordered systems with localized defect and edges states in both sublattices [30]. The magnitudes of HFIs are minimized and maximized in the cases of ferromagnetic and antiferromagnetic electron spin distributions, respectively.

Many carbon nanostructures of reduced dimensionality (e.g. nanotubes and fullerenes) represent non-planar topologies. Local curvatures lead to the sp^2-sp^3 rehybridization of carbon atoms and enable a Fermi contact interaction involving the electron spins of π states [31]. This results in a positive contribution of the π states unless n^c is close to zero: a contribution due to the NN spin-polarization effect is negative in this case. The degree of rehybridization m of the π states ($s^m p$)

TABLE II: Hyperfine coupling constants for three general cases of spin populations n^c of the carbon atoms of A and B sublattices of graphene.

	$A_{iso}(\text{A})/n^c$	$A_{iso}(\text{B})/n^c$	$A_{dip}(\text{A})/n^c$	$A_{dip}(\text{B})/n^c$
$n_A^c=n_B^c>0$	-38	-38	65	65
$n_A^c>0; n_B^c=0$	135	-173	116	-52
$n_A^c=-n_B^c>0$	308	-308	168	-168

can be described using a local bond angles analysis [32]. For the case of large curvature radii the original expression for m can be reformulated in a more convenient form, $m=d_{cc}^2/8(1/R_1+1/R_2)^2$, where d_{cc} is the C–C distance, R_1 and R_2 are the principal curvature radii. The curvature-induced contribution to the Fermi contact ^{13}C HFCC is then $A_{iso}^{curv}=\frac{8\pi}{3}\gamma_e\gamma_I\hbar^2nm\phi_{2s}^2(0)$, where $\phi_{2s}(0)$ is the magnitude of the carbon atomic $2s$ wavefunction at the point of nucleus. For a 1.4 nm diameter carbon nanotube $A_{iso}^{curv}/n^c \approx 8.7$ MHz, a value that is smaller than the spin-polarization contributions for all scenarios given in Tab. II. However, the curvature-induced direct coupling grows as R^{-2} with decreasing R and becomes significant, e.g. in the case of ultranarrow ($d < 1$ nm) carbon nanotubes [28].

Since the natural abundance of the “HFI-active” ^{13}C isotope is small ($\approx 1\%$), consideration of the nuclei of other elements is important for a complete description of HFIs in carbon nanostructures. The common substitution impurities are boron and nitrogen with all natural isotopes having nuclear spins. Graphene edges can be terminated by hydrogen and fluorine atoms with both ^1H and ^{19}F spin-1/2 nuclei (99.9885% and 100% natural abundance, respectively) having high gyromagnetic ratios ($\gamma(^1\text{H})/\gamma(^{13}\text{C}) \approx \gamma(^{19}\text{F})/\gamma(^{13}\text{C}) \approx 4$). I consider HFIs in a reduced set of molecular fragments (only 3- and 4-ring structures included) with impurities and edge functionalizations in all possible positions. The calculated HFCCs have been fitted to the Karplus-Fraenkel relation, with no Δr terms included (Tab. III). Both Fermi contact and dipolar HFCCs of the impurity nuclear spins show a monotonous increase along the $^{11}\text{B}-^{13}\text{C}-^{14}\text{N}$ series when compared to the results for ^{13}C HFCCs (Tab. I). The NN relative spin-polarization effects (a/c ratio) on the Fermi contacts HFCCs tend to decrease along the series. While the HFIs of the nuclear spins in substitution impurities are highly anisotropic, the hyperfine couplings of the edge nuclei show small anisotropy due to the sp^3 character of bonding. When ^1H and ^{19}F edge nuclei are bound to the C_{sp^2} atoms, the isotropic HFCCs are of the same order of magnitude as those of the ^{13}C spins in the graphene lattice. The influence of the NN carbon atoms (second NNs to the terminating atom) is very similar for ^1H and ^{19}F nuclei and smaller than in the case of ^{13}C HFCCs ($a_H/c_H \approx a_F/c_F \approx -6$). The spin polarization effect on ^{19}F HFCCs is stronger

TABLE III: Parameters (in MHz) describing the HFIs of nuclei of substitutional impurities (^{11}B and ^{14}N), monoatomic functional groups (^1H and ^{19}F) and rehybridized carbon atoms (^{13}C) at the edges.

Nucleus	Position	A_{iso}		A_{dip}	
		a	c	a	c
^{11}B	subst. impurity	43	-31	60	6
^{14}N	subst. impurity	150	-22	130	-10
^1H	C_{sp^2} edge	-118	20		
^{19}F	C_{sp^2} edge	240	-40		
^1H	C_{sp^3} edge		350		
^{19}F	C_{sp^3} edge		750		
^{13}C	C_{sp^3} edge		-68		

and of the opposite sign compared to that of protons ($a_F/a_H \approx c_F/c_H \approx -2$). When edge atoms are bound to the rehybridized (sp^3) carbon atoms, n^c is zero but the NN contribution is significantly enhanced. The NN contribution to the ^{13}C hyperfine coupling of the sp^3 edge carbon atom itself ($c = -68$ MHz) has a similar magnitude as that of the sp^2 edge atoms ($c = -57$ MHz). HFIs with the boundary spins (H-terminated edges are often obtained in experiments [33]) have to be taken into account when designing carbon-based nanoscale devices for spintronics or quantum computing. A chemical modification of the graphene edges (e.g. substitution of the hydrogen atoms by alkyl-groups) can be suggested to reduce unwanted effects from the HFIs with boundary spins.

In conclusion, the results of first principles calculations show that the hyperfine interactions in graphene and related nanostructures are defined by the local distribution of the conduction electron spins and by the local atomic structure. A complete set of parameters describing the hyperfine interactions with the extended Karplus-Fraenkel expression was determined for the ^{13}C and other common nuclear spins. These results will permit to control the magnetic interactions between the spins of electrons and nuclei by tailoring the chemical and isotopic compositions, local atomic structures, and strain fields in sp^2 carbon nanostructures. Some practical recipes for minimizing interactions with nuclear spins are given.

I acknowledge D. Loss and Yu. G. Semenov for motivating discussions, and L. Helm and I. Tavernelli for comments on this manuscript. I also thank the Swiss NSF for financial support and CSCS Manno for computer time.

* Electronic address: oleg.yazyev@epfl.ch

[1] I. Žutić, J. Fabian, and S. Das Sarma, Rev. Mod. Phys. **76**, 323 (2004).

[2] D. Loss and D. P. DiVincenzo, Phys. Rev. A **57**, 120 (1998).

[3] B. E. Kane, Nature **393**, 133 (1998).

[4] Z. H. Xiong, D. Wu, Z. V. Vardeny, and J. Shi, Nature **427**, 821 (2004).

[5] S. D. Bader, Rev. Mod. Phys. **78**, 1 (2006).

[6] K. Tsukagoshi, B. W. Alphenaar, and H. Ago, Nature **401**, 572 (1999).

[7] S. Sahoo, T. Kontos, C. Schönenberger, and C. Sürgers, Appl. Phys. Lett. **86**, 112109 (2005).

[8] L. E. Hueso, J. M. Pruneda, V. Ferrari, G. Burnell, J. P. Valdés-Herrera, B. D. Simons, P. B. Littlewood, E. Artacho, A. Fert, and N. D. Mathur, Nature **445**, 410 (2007).

[9] E. W. Hill, A. K. Geim, K. Novoselov, F. Schedin, and P. Blake, IEEE Trans. Magn. **42**, 2694 (2006).

[10] M. Bockrath, W. Liang, D. Bozovic, J. H. Hafner, C. M. Lieber, M. Tinkham, and H. Park, Science **291**, 283 (2001).

[11] M. R. Buitelaar, A. Bachtold, T. Nussbaumer, M. Iqbal, and C. Schönenberger, Phys. Rev. Lett. **88**, 156801 (2002).

[12] B. Trauzettel, D. V. Bulaev, D. Loss, and G. Burkard, cond-mat/0611252.

[13] P. G. Silvestrov and K. B. Efetov, Phys. Rev. Lett. **98**, 016802 (2007).

[14] Y. G. Semenov, K. W. Kim, and G. J. Iafrate, Phys. Rev. B **75**, 045429 (2007).

[15] A. V. Khaetskii, D. Loss, and L. Glazman, Phys. Rev. Lett. **88**, 186802 (2002).

[16] J. M. Taylor, C. M. Marcus, and M. D. Lukin, Phys. Rev. Lett. **90**, 206803 (2003).

[17] R. J. Epstein, F. M. Mendoza, Y. K. Kato, and D. D. Awschalom, Nat. Phys. **1**, 94 (2005).

[18] L. Childress, M. V. G. Dutt, J. M. Taylor, A. S. Zibrov, F. Jelezko, J. Wrachtrup, P. R. Hemmer, and M. D. Lukin, Science **314**, 281 (2006).

[19] The Gaussian03 code [M. J. Frisch *et al.*, Gaussian03, Rev. C.02, Gaussian, Inc., Wallingford, CT, 2004] was used.

[20] N. Rega, M. Cossi, and V. Barone, J. Chem. Phys. **105**, 11060 (1996).

[21] A. D. Becke, Phys. Rev. A **38**, 3098 (1988); C. Lee, W. Yang, and R. G. Parr, Phys. Rev. B **37**, 785 (1988); A. D. Becke, J. Chem. Phys. **98**, 5648 (1993).

[22] L. Hermosilla, P. Calle, J. M. García de la Vega, and C. Sieiro, J. Phys. Chem. A **109**, 1114 (2005).

[23] J. R. Bolton and G. K. Fraenkel, J. Chem. Phys. **40**, 3307 (1964); D. J. M. Fassaert and E. de Boer, Recl. Trav. Chim. Pays-Bas **91**, 273 (1972); R. F. Claridge, C. M. Kirk, and B. M. Peake, Aust. J. Chem. **26**, 2055 (1973).

[24] M. Karplus and G. K. Fraenkel, J. Chem. Phys. **35**, 1312 (1961).

[25] K. Nakada, M. Fujita, G. Dresselhaus, and M. S. Dresselhaus, Phys. Rev. B **54**, 17954 (1996).

[26] H. Overhof and U. Gerstmänn, Phys. Rev. Lett. **92**, 087602 (2004).

[27] J. Conard, H. Estrade, P. Lauginie, H. Fuzellier, G. Furdin, and R. Vasse, Physica B **99**, 521 (1980).

[28] O. V. Yazyev and L. Helm, Phys. Rev. B **72**, 245416 (2005).

[29] K. Kelly and N. Halas, Surf. Sci. **416**, L1085 (1998).

[30] O. V. Yazyev and L. Helm, cond-mat/0610638.

[31] C. H. Pennington and V. A. Stenger, Rev. Mod. Phys. **68**, 855 (1996).

[32] R. C. Haddon, J. Am. Chem. Soc. **108**, 2837 (1986).

[33] Y. Kobayashi, K. Fukui, T. Enoki, and K. Kusakabe, Phys. Rev. B **73**, 125415 (2006).